


**Nanoscale photoemission from a focused propagating surface plasmon**Guiqi Wang, Peng Lang, Yulu Qin, Boyu Ji <sup>\*</sup>, Xiaowei Song, and Jingquan Lin<sup>†</sup>*School of Science, Changchun University of Science and Technology, Changchun 130022, People's Republic of China*

(Received 1 May 2021; accepted 10 September 2021; published 27 October 2021)

Propagating surface plasmons (PSPs) provide an important platform for designing various photoelectric devices such as nanometer-confined ultrafast electron sources. Here, we investigate the nanoscale photoemission from a focused PSP hot spot using time-of-flight photoemission electron microscopy. It is found that the induced photoelectrons from the focused PSP exhibit an obvious feature of the above threshold photoemission process, while the photoelectron spectra from a local surface plasmon (LSP) under the same illumination condition exhibit a characteristic of thermally assisted multiphoton photoemission. In addition, results show that the measured photoelectron yield from the focused PSP region is nearly one order of magnitude higher than that from the LSP region, and we found this is contrary to the calculation results that the yield from the LSP is much higher than that from the focused PSP when the local field intensity and plasmon lifetime of the two plasmonic modes are included. The large discrepancy in the photoelectron energy spectra, as well as in the measured and calculated photoelectron intensity between the focused PSP and LSP, can be attributed to the existence of different decay channels between the two plasmonic modes. This paper provides a deep understanding of the photoemission mechanism induced by plasmon effects, and it shows that the focused PSP is promising as a robust nanoscale electron source which can supply energetic and higher flux electron emission.

DOI: [10.1103/PhysRevB.104.155432](https://doi.org/10.1103/PhysRevB.104.155432)**I. INTRODUCTION**

Plasmon effects have become a promising platform for enhanced photoemission due to the dramatically near field enhancement and spatial confinement [1,2]. Localized surface plasmons (LSPs) supported by nanoparticle arrays or nanoscale tips have been utilized to improve the photoemission performance of the ultrafast electron sources [1–7]. The LSP-based ultrafast electron source is potential to the field of free electron laser, ultrafast electron microscopy, and other photoelectric applications, where it requires not only high brightness but also a small emission area to ensure a high spatial resolution. However, the large lateral size and easy degradation (due to sharp edges) for the nanoparticle arrays as well as the always accompanying high bias voltage for the nanotip will seriously hinder their direct application to these above mentioned fields [8,9].

Propagating surface plasmons (PSPs) as an electromagnetic mode propagating along the interface of the metal/dielectric or vacuum interface can be focused by PSP lens to a volume far below the diffraction limit with high local field enhancement [10,11]. Accordingly, on one side, the associated photoemission from the focused PSP is at nanometer scale [12,13]; on the other side, the flat surface which supports the focused PSP is robust due to its independence from nanostructures such as sharp edges, tips, and protrusions that easily suffer from degradation with intense laser illumination [13]. Recently, the focused PSP has been suggested to be a good candidate for the high brightness nanoscale photoemis-

sion source with a high repetition rate [12,13]. It is known that the photoelectron spectrum is critical for revealing the underlying photoemission mechanism. As far as we know, the only research on photoelectron spectra induced by the focused PSP has been reported in Ref. [12], where a concentric metallic rings scheme was utilized. However, a single homogeneous nanoscale plasmonic focal spot, which is critical to the building of nanoscale electron sources, is difficult to be achieved in this kind of concentric metallic rings scheme due to the destructive interference between counterpropagating surface plasmon polariton (SPP) waves [14,15]. Moreover, the role of collective modes such as PSP or LSP for photoemission under ultrashort laser pulse excitation with photon energies well below the work function is still controversially discussed in literature [16–21], and this needs further works to clarify.

In this paper, we report the photoemission induced by a single homogeneous focused PSP focal spot on an Au plane illuminated by an obliquely incident femtosecond pulse using time-of-flight photoemission electron microscopy (ToF-PEEM). A ToF-PEEM with high energy and spatial resolution is a significantly powerful tool to characterize the photoelectron spectrum in the nanometer scale. Thanks to the high spatial and energy resolution ability of the PEEM, we are able to characterize the nanoscale photoelectron emission from a focused PSP. We found there is an obvious difference in the photoelectron spectrum between the focused PSP and LSP under the same laser incident conditions. Furthermore, we also found that the photoemission intensity is not only strongly related to the near field enhancement and the duration time of the plasmon, but also determined by the decay channels of the plasmonic mode.

<sup>\*</sup>jiboyu@cust.edu.cn<sup>†</sup>linjingquan@cust.edu.cn

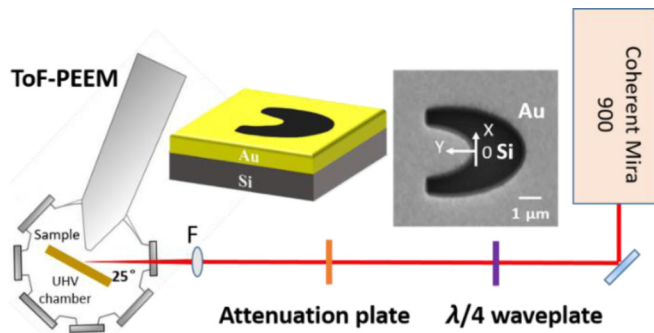


FIG. 1. Schematics of the experimental setup.

## II. EXPERIMENTAL SETUP

Figure 1 shows the schematic diagram of the experimental setup. ToF-PEEM with better than 40-nm lateral resolution and 50-meV energy resolution is used to measure the photoelectron spectrum from an Au film excited by the focused femtosecond PSP. The light source is a mode-lock Ti-sapphire laser oscillator (Coherent, Mira 900) delivering laser pulses with a duration of nearly 150 fs at a repetition rate of 76 MHz and tunable center wavelength from 700 to 900 nm. The linearly polarized light pulses can be tuned to generate a circularly polarized light pulse by passing through a  $\lambda/4$  plate, and an attenuation plate is used to adjust the power of incident pulses. The sample is illuminated by the incident laser pulse at  $65^\circ$  to the normal of the sample, and the incident pulse is focused on the sample surface with a spot size of around  $40 \times 80 \mu\text{m}$ .

A PSP focusing lens used for the oblique excitation in our case is designed to compensate for the phase delay to focus the generated PSP fields when the incident wavelength is 800 nm [10,22]. The structure is designed as semielliptical geometry with long ( $y$ -axis) and short ( $x$ -axis) diameters of 4 and  $2 \mu\text{m}$ , respectively. The PSP focusing lens is fabricated by focused ion beam technology, and the trench is etched in a 200-nm-thick Au film coated on Si substrate. The schematic diagram and scanning electron microscope image of the PSP focusing lens are shown in the insets of Fig. 1.

The numerical computations of the focused PSP and LSP near field are carried out by the software FDTD method; the exact dimensions of FDTD are set as  $8000 \times 10\,000 \times 1340 \text{ nm}$ ; and the perfect matched layer boundary condition is used in  $x$ ,  $y$ , and  $z$  directions. The mesh size is  $2 \times 2 \times 2 \text{ nm}$  in the region of the plasmonic lens. The optical properties of Au are obtained using the data from Johnson and Christy [23]. The circularly polarized pulse is composed of two orthogonally polarized linearly polarized plane waves, the phase difference of which is  $\pi/2$ ; this setting is widely used by others for FDTD [22,24]. The pulse duration is 150 fs. The incident pulse is at  $65^\circ$  to the normal of the sample to mimic PEEM illumination geometry.

## III. RESULTS AND DISCUSSION

Figure 2(a) shows the PEEM image of the plasmon lens illuminated by a  $p$ -polarized 800-nm pulse. The PSP is excited at the edge of the trench by the femtosecond light pulse and then focused by the PSP focusing lens; the PSP converges at the focus of the lens denoted by the red circle. We measured

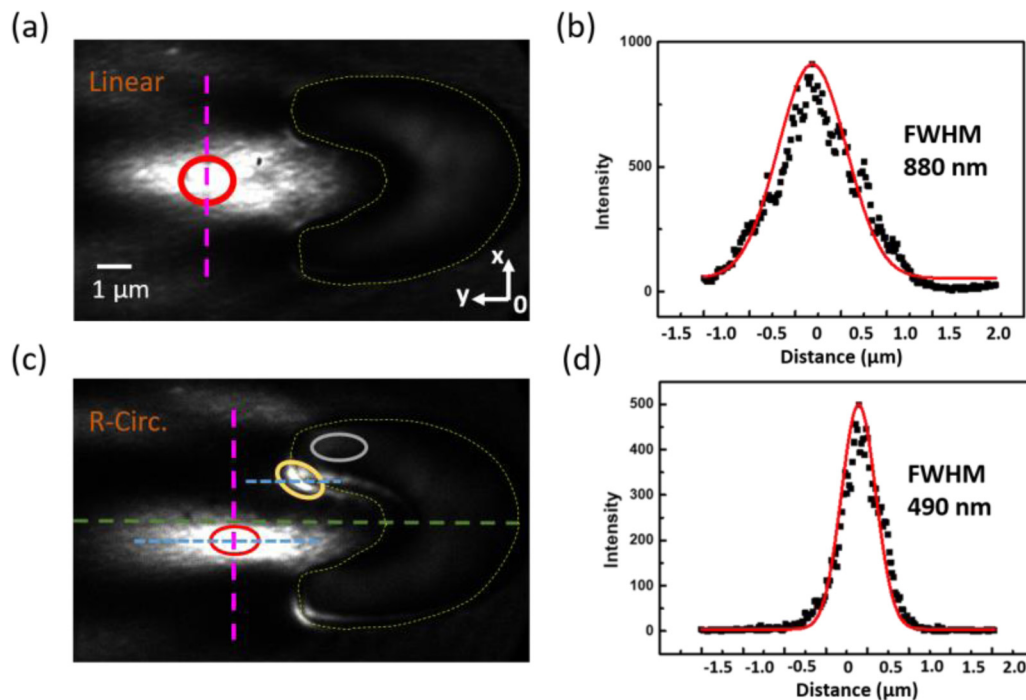


FIG. 2. (a) PEEM image of a plasmon focusing lens illuminated by 800-nm  $p$ -polarized femtosecond light. (b) The photoemission intensity profile excited by focused PSP along the pink dashed line shown in Fig. 2(a); the red line is obtained by Gaussian fitting. (c) PEEM image of a PSP focusing lens illuminated by 800-nm right circularly polarized femtosecond light. (d) The photoemission intensity profile excited by focused PSP along the pink dashed line shown in Fig. 2(c); the red line is obtained by Gaussian fitting.

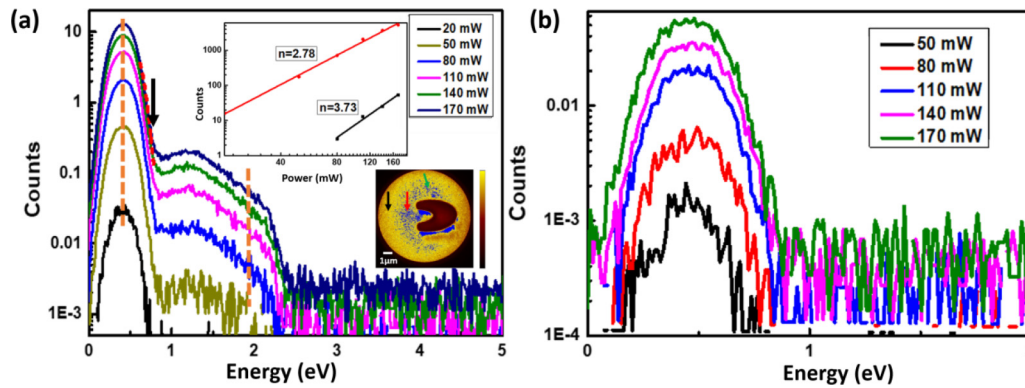


FIG. 3. (a) The measured photoelectron spectra at a focus spot denoted by the red circle in Fig. 2(c); the upper left inset is the measured photoelectron yield at 0.4 and 1.9 eV as a function of incident power, respectively. The lower right inset is the one-order-of-magnitude linear photoemission UV-PEEM image of the sample illuminated by Hg lamp. (b) The measured photoelectron spectra on the Au plane without the effect of PSP at varied incident powers.

photoemission intensity profiles of the focused PSP excited by the linearly polarized laser pulse along the vertical pink dashed line in the  $x$  direction in Fig. 2(a), and the result is shown in Fig. 2(b) (the black dots); it is then fitted by a Gaussian function as shown by the red line; we obtained that the full width at half maximum (FWHM) of the focused PSP is around 880 nm, which is close to the scale of the incident wavelength. We further reduce the focusing spot by tailoring the incident laser pulse. The PEEM image of the excited PSP by right circularly polarized light as an example is shown in Fig. 2(c). The PEEM image presents distinctly asymmetric distribution with the focusing of the PSP slightly below the central axis of the lens structure (green dashed line). Similar phenomena with asymmetric distribution of an excited PSP have also been observed by others and explained by the plasmonic spin-Hall effect [22,24]. The measured photoemission intensity profile of the focused PSP excited by a right circularly polarized laser pulse along the vertical pink dashed line in the  $x$  direction as denoted in Fig. 2(c) is shown in Fig. 2(d). It shows that the obtained FWHM of the focused PSP by Gaussian fitting is only 490 nm, around half of the incident wavelength. This result shows that a much more tightly focused nanoscale spatial manipulation of photoemission is achieved by the circularly polarized laser pulses. As the right circularly polarized light pulse excitation provides a much smaller photoemission hot spot and it becomes much more interesting for the nanoscale ultrafast electron source, we focus attention on the photoemission characteristics of the focused PSP excited by a right circularly polarized laser pulse in the following.

The photoelectron spectra from the focus spot region denoted by the red circle in Fig. 2(c) under right circularly polarized laser excitation with different incident powers are shown in Fig. 3(a). For the photoelectron spectrum with 170-mW laser illumination, the Fermi edge is clearly visible and is fitted perfectly by a Fermi function as denoted by the red dotted line where a black arrow marks the Fermi level position at  $E_F = 0.65$  eV. The measured photoelectron spectra obtained from the Au plane without the PSP focusing lens [the measured position is marked with a green arrow in the lower right inset in Fig. 3(a)] but under the same experimental conditions are shown in Fig. 3(b) as a reference. By comparing

the spectra with and without the lens, it can be found that the spectra from the Au plane with the PSP focusing lens are quite different from those obtained from the Au plane without the PSP focusing lens. The spectra in Fig. 3(a) present a higher cutoff of energy reaching to around 2.3 eV and there appears a plateau in the photoelectron spectrum with the increase of power to 80 mW and above. It is known that a classic above threshold photoemission (ATP) process behaves as multiple peaks or plateaus separated by the incident photon energy in the energy spectrum [25]. This plateau profile in the spectrum in Fig. 3(a) is reminiscent of the ATP process in our case. To prove this claim, we further measured the electron yield corresponding to 0.4-eV position as a function of incident power; the measured results are shown as a red line in the upper left inset in Fig. 3(a). The slope of 2.78 indicates that the photoemission at 0.4-eV position is a three-photon photoemission process. We further obtained the work function of Au material by  $\phi(\text{Au}) = 3h\nu - E_F$ , where  $\phi(\text{Au})$  is the work function of Au,  $h\nu$  is the photon energy, and  $E_F$  is the Fermi energy. The result denotes that the work function of the Au plane with the PSP focusing lens is only 4 eV, which is much less than the usual work function of Au: 4.6–5.1 eV [26]. The lower right inset in Fig. 3(a) shows the one-photon photoemission PEEM image illuminated by Hg lamp. It can be seen that the central area denoted by the red arrow is slightly brighter than the surrounding area denoted by the black arrow, which indicates the decrease of the work function in the central area. We attribute the decrease of the work function of the Au plane to the focused ion beam (FIB) fabrication: the ion beam provides the energy to permanently adsorb chemicals that are present [27]. The electron yield of 1.9 eV as a function of the incident power as a black line is shown in the upper left inset in Fig. 3(a). The slope of 3.73 indicates that the photoemission at 1.9 eV is a four-photon photoemission process. Noticeably, the slopes increase from 3 to 4 in the photoelectron spectra from the peak position of 0.4 eV to the plateau of 1.9 eV, and it is also noted that the energy difference between 0.4 and 1.9 eV is approximately equal to the energy of an incident photon (1.55 eV). This result clearly shows that the higher-energy electrons at 1.9 eV are emitted by the absorption of an extra photon for emission, i.e., an ATP process at a high kinetic-energy regime [28].

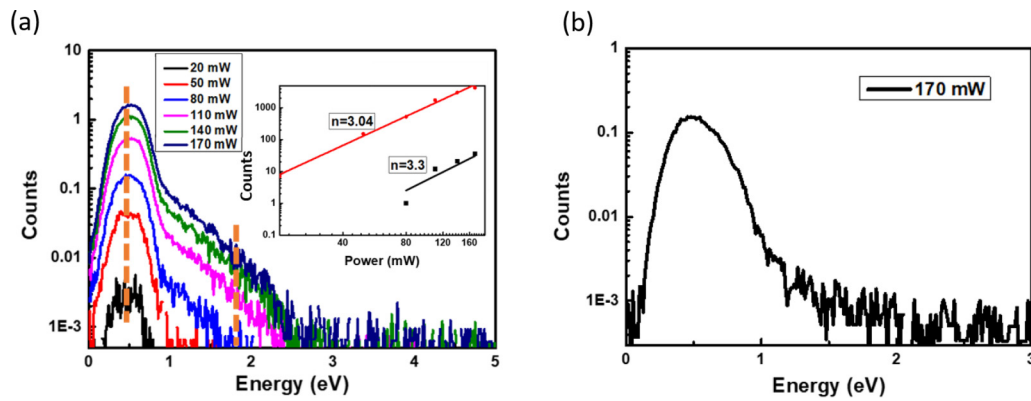


FIG. 4. (a) The photoelectron spectra from the LSP with different incident powers. The inset shows the measured photoelectron yield at 0.4 and 1.9 eV as a function of incident power, respectively. (b) The photoelectron spectrum from the Si substrate with 170-mW femtosecond laser illumination.

Therefore, the results demonstrate that an ATP process is achieved at the focal point of the PSP focusing lens on the Au plane.

It is interesting to note that an extra hot spot around the upper rim of the lens as denoted by a yellow circle in Fig. 2(c) is observed in the PEEM image under the right circularly polarized laser excitation. To prove the electron emission pattern on the rim in this paper is a localized mode, we calculated the wavelength-dependent near field enhancement spectrum of the localized hot spot on the rim via FDTD simulation; the simulated near field spectrum exhibits a resonant peak at around 800 nm (as depicted in Fig. S1 in Supplemental Material [29]; see also Ref. [30] and references therein). Moreover, we also use left circularly polarized laser pulses to illuminate the sample, and a hot spot appears on the lower rim of the lens structure, the position of which is symmetrical to the case of a right circularly polarized laser pulse; in addition, when the sample is illuminated by the linearly  $p$ -polarized light, two hot spots, which are symmetric along the  $y$  axis (the main axis of the structure), can be observed (as depicted in Fig. S2 in Supplemental Material [29]; see also Refs. [10,31–33] and references therein). The resonant feature and symmetric appearance of the hot spots on the rim when irradiated by different polarization states' laser pulses confirm that the electron emission pattern on the rim as denoted by the yellow circle in Fig. 2(c) is a localized plasmon mode rather than a tip-induced field enhancement (such as the lightning rod effect).

The simultaneous appearance of the LSP in the structure brings our attention to measure photoemission from the LSP, and leads us to investigate the possible difference in photoemission between the nanoscale hot spot formed by the focused PSP and hot spot (LSP) on the rim of the lens structure under the same illumination conditions. Therefore, the photoemission characteristic induced by the LSP was explored. The measured photoelectron spectra of the hot spot induced by the LSP with varied incident powers are shown in Fig. 4(a). It can be seen that energy spectra corresponding to the LSP show an obvious difference in the higher-energy section from those of the focused PSP as shown in Fig. 3(a). The plateau that indicates an ATP effect in Fig. 3(a) disappears in Fig. 4(a), and it is replaced by an almost smooth linear decrease without the

feature of ATP. A linear decrease represents an exponential drop of the electron distribution, which is expected for the high-energy tail of a Fermi distribution resulting from thermal effects involved in the photoemission process [34]. We also measured the photoelectron yield as a function of incident powers at 0.4 and 1.9 eV, respectively, as shown in the inset of Fig. 4(a). The measured slopes show that they both correspond to three-photon photoemission processes. This phenomenon further reveals that the photoelectron induced by the LSP was not mainly through an ATP process. The kinetic energy of electrons being higher than three photons is most probably due to the multiphoton photoemission that is assisted by the thermal effect [25,35]. The maximum electron temperature induced by the LSP and PSP can reach 4700 and 1400 K, respectively, based on the calculation using the two-temperature model [36], and it shows that the electron temperature induced by the LSP is almost 3.36 times higher than that induced by the PSP. Additionally, 4700 K in the LSP case implies sufficiently high transient electronic temperatures to promote contributions from the thermally assisted effect [37]. Therefore, the observed thermally assisted multiphoton process in Fig. 4(a) is mainly attributed to the higher electron temperature in the LSP region.

Furthermore, to rule out the possibility that the differences in the spectra for Figs. 3(a) and 4(a) are due to different gold surface properties on the planar film and on the rim, we selected several regions along the rim with lower yield than the hot spot used for obtaining the spectra in Fig. 4(a) and extracted the photoelectron spectra (as depicted in Fig. S3 in Supplemental Material [29]). Meanwhile, we compared the spectra from those lower electron yield regions on the rim with those from a region of flat gold film as shown in Fig. 3(b); they show that the thermally assisted behaviors for the selected lower photoelectron yield regions from the rim have disappeared, and they show a very similar behavior as that from the region in the flat film used for Fig. 3(b), indicating that the differences in the spectra of the LSP hot spot in Fig. 4(a) and focused PSP region in Fig. 3(a) are not due to different gold surface properties on the planar film and on the rim.

To further confirm the thermally assisted multiphoton photoemission process in Fig. 4(a), we rule out some other

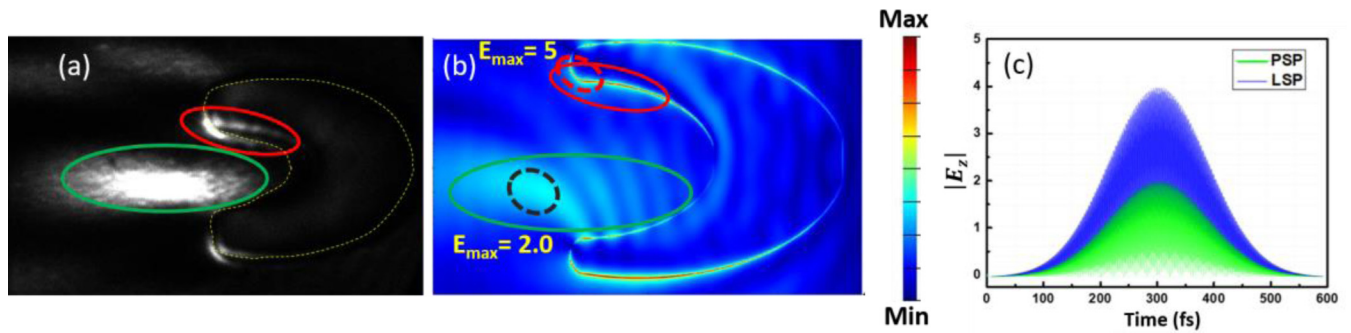


FIG. 5. (a) The extraction regions of the yield induced by LSP (red circles) and PSP (green circles) in the experiment. (b) The simulated  $|E_z|$  of near field distribution illuminated by right circularly polarized light by FDTD. (c)  $|E_z|$  as a function of time for LSP and PSP, respectively.

possible origins and mechanisms. Due to the limitation of the spatial resolution of the ToF-PEEM, it was inevitable to obtain the electrons coming from the Si substrate when we extracted the electrons emitted from the LSP hot spot located on the edge of the lens. To exclude the dominated effect of the electrons emitted from the Si substrate to the photoelectron spectra of the LSP hot spot, we exclusively obtained the photoelectron spectrum of the Si substrate with 170-mW laser illumination as shown in Fig. 4(b). The extracted area is denoted by the gray circle in Fig. 2(c) where photoemission is only from the Si substrate (Au film was etched through the Au film for the fabrication of the lens). It can be seen that the cutoff of the energy is only around 1.5 eV, which is far less than the cutoff energy around 2.5 eV of the LSP hot spot spectrum at 170 mW in Fig. 4(a). Therefore, the possibility of Si substrate emitted electrons dominating the spectra of the LSP hot spot can be ruled out and most photoelectrons are contributed by the LSP. Further, the field emission is also excluded. It is known that Keldysh parameters as shown in Eq. (1) can be used to identify the photoemission mechanism in the multi-photon regime or in the strong field regime [38]:

$$\gamma = (\omega\sqrt{2m\phi}/eE) \quad (1)$$

where  $\omega$  is the laser frequency,  $\phi$  is the work function of the material,  $E$  is the electric field intensity, and  $e$  and  $m$  are the charge and mass of the electron. Considering the near field enhancement factor simulated by FDTD simulation, the corresponding Keldysh parameter is  $\gamma \sim 16 > 1$ , suggesting that the field emission effect can be ruled out.

It is important to evaluate the photoelectron intensity from the nanoscale spot formed by focusing the PSP. Towards this end, we also compare the photoelectron intensity from the focused PSP and LSP. We measured the total photoelectron yields from the LSP region (denoted by a red solid line ellipse) on the rim and focused PSP region (denoted by a green solid line ellipse) near the focusing point of the lens as shown in Fig. 5(a). The experimental results show that the photoelectron yield induced by the PSP is almost one order of magnitude higher than that induced by the LSP. In the following, we calculated photoelectron yields corresponding to the same areas of the two regions for the LSP and focused PSP by FDTD simulation [also marked with the same sized red and green solid line ellipses in Fig. 5(b)]. Considering the nonlinear dependent relation between the photoelectron yield

and the electric field  $Y \propto E_z^{2n}$  [1,3], where  $n$  is nonlinear order (here  $n = 3$ ), thus the photoelectron yield that includes both the intensity and plasmon duration time of the near field can be calculated using Eq. (2):

$$Y \propto \iint E_z^6 dt ds \quad (2)$$

where  $Y$  and  $E_z$  correspond to the photoelectron yield and  $z$  component of the near field, respectively. Area  $s$  corresponds to the whole region denoted by the red and green ellipses in Fig. 5(b). It is known that the photoemission intensity is closely related to the  $E_z$  component of the near field intensity [39]. The  $E_z$  component of the near field distribution of the PSP focusing lens illuminated by right circularly polarized light is simulated by FDTD, a two-dimensional field monitor in the  $x$ - $y$  plane ( $z = 0$  nm) was set, and the result is shown in Fig. 5(b). It is noted that there is no interference fringe in the measured PEEM pattern as shown in Fig. 5(a), but the FDTD simulation of electric field distribution in Fig. 5(b) exhibits fringes. We attribute this discrepancy to the high order nonlinear dependence of photoelectron yield on the  $E_z$  component of the PSP field. We follow the method that connects the photoelectron distribution to the temporal integral of the sixth power of the instantaneous electric field to reproduce the PEEM image [27,40]. The reconstructed PEEM image shows that the interference fringes disappear (as depicted in Fig. S4 in the Supplemental Material [29]; see also Refs. [27,40] and references therein). In addition, the PSP and LSP are two kinds of plasmonic modes [41–43] and  $t$  is the duration time of the plasmon near field. To obtain the duration time  $t$  of the LSP and the PSP, respectively, two time point monitors were set at the surface ( $z = 0$  nm) of the sample to capture the time evolution of the plasmon near field by FDTD simulation: one of them was set at 4-nm distance away from the edge to monitor the LSP, and the other one was set at the focus of the PSP. The temporal evolutions of the electric field of the LSP and PSP are displayed in Fig. 5(c). The calculated results from Eq. (2) show that photoemission yields in the corresponding LSP and focused PSP regions are about  $2.0 \times 10^7$  and  $2.3 \times 10^6$ , respectively. In contrast to the experimental results, it shows that the calculated yield of the LSP is about one order of magnitude higher than that of the PSP. Combining the experimental and simulation results, it shows that the difference in photoelectron yield between experimental and simulation reaches to nearly two orders of

magnitude. The obvious contradiction in photoelectron yield between the experimental and simulation results indicates that the measured photoelectron yield difference between the LSP and focused PSP regions cannot be fully explained by only including effects of the near field intensity and the plasmon lifetime.

Our experimental results show that a focused PSP excites an obvious ATP process while the LSP does not. Also, a large discrepancy exists between the calculation and experimental measurement of photoelectron yield for the focused PSP and LSP. The above two differences cannot be explained by considering the combined factors of local field and plasmon lifetime. Both experimental results suggest there should be other physical reasons responsible for the explanation of the difference.

The observed difference in photoelectron energy profile and the higher photoemission yield from the focused PSP than that from LSP under the same illumination conditions may result from different decay channels between PSP and LSP modes. It is known that there are two paths for plasmons to damp: radiative and nonradiative paths [44]. The LSP can damp through both radiative and nonradiative paths. In contrast, the PSP is a kind of subradiative mode, which means nearly all PSP quanta will decay through nonradiative transition [45,46]. The LSP damp through both radiative and nonradiative paths indicates that parts of LSP quanta will decay by regenerating photons, which has no contribution to photoelectron emission [47]; that the PSP only decays through nonradiative transition means all the decay can play a role in photoemission [17,19,48]. As a result, the different channels between PSP and LSP modes can be important factors responsible for much higher photoelectron yield from the focused PSP region even though the calculated photoelectron yield from the LSP region is about one order of magnitude higher than that from the focused PSP region when only the local field intensity and the lifetime of the two modes are included.

Furthermore, photoelectron spectra of the focused PSP exhibit an obvious ATP feature while the LSP spectra do not. This difference in the spectrum between the focused PSP and LSP can also be attributed to different decay channels of the PSP and LSP. When the plasmon is excited, plasmon decay takes place on a femtosecond timescale from two paths, either the radiative path through reemitted photons or the nonradiative path by transferring the energy to hot electrons [44]. As discussed above, in the radiative process, the energy that decays by reemitted photons has no contribution to photoelectron emission. While in the nonradiative process the plasmon first decays into single-electron excited states, this will excite photoemission if the energy of the excited electron exceeds the work function of the material. The LSP can decay in both radiative and nonradiative damping paths; part of the energy will transfer to reemitted photons. In contrast, the PSP will only decay through a nonradiative damping path [45,46]; the energy will dominantly transfer to excite the photoelectrons. The results of a higher local field but a limited maximum photoemission intensity in the LSP are evidence that radiative decay may be dominating, thus not favoring the absorbed energy to decay through photoemission [48]. In other words, by appropriately selecting the plasmonic mode, it is possible to efficiently promote plasmon damping via specific channels

[44], moving from the radiative losses to the generation of hot electrons as a primary decay channel [17], and a strongly enhanced photoemission process can be predicted. Moreover, as more PSP quanta can exist in the excited state than LSP quanta during the incident pulse duration of 150 fs due to the longer dephasing time of a PSP (roughly 100 fs) compared with the LSP (roughly several to less than 20 fs) [43], the probability for electrons to absorb PSP quanta will be higher than for the absorbing LSP quanta. Therefore, it can be qualitatively concluded that PSP excitation is more efficient for energy utilization to excite photoelectron emission and easier to induce an ATP effect than LSP excitation.

Furthermore, the dominated thermally assisted multiphoton photoemission in the photoelectron emission induced by the LSP as observed in Fig. 4(a) can be attributed to the stronger energy concentration of the LSP [34,35,49,50]. As shown in Fig. 5(b), a higher near field enhancement of the LSP will accompany a stronger heating to electron gas with a calculated maximum electron temperature of 4700 K in our case during the laser pulse illumination. This leads to a fast thermalization and a broadened electron distribution around the Fermi edge. As a result, the heated electron gas will be emitted during the laser pulse illumination and the thermally assisted photoemission becomes significant [49,50]. Moreover, the LSP excited on the nanoscale sharp rim of the structure can concentrate the energy into a much smaller volume than that of the focused PSP on the Au plane, and this can be observed in the PEEM image as shown in Fig. 2(c). Therefore, the higher-energy density of the LSP on the rim of the structure correlates with a region of much higher electron gas temperature [34], resulting in thermally assisted multiphoton photoemission.

Lastly, we noticed a similar work that utilized a circular grating coupler to focus the SPP to the center of the ring for the generation of photoelectrons [12]. In Ref. [12], the authors demonstrated the unambiguous distinction between optically triggered electron emission (photoemission) and purely plasmonic field triggered electron emission (termed “plasmoemission”). Reference [12] shows a fifth order photoemission process while our paper shows only a fourth order process. This is mainly due to the fact that the diameter of the circular grating coupler in Ref. [12] is 40  $\mu\text{m}$ ; however, in our paper, the long axis of a moon sickle shaped structure is only 4  $\mu\text{m}$ . Therefore the circular grating coupler can collect more energy from the incident laser pulse, and thus it is favorable for obtaining a higher SPP field intensity, which results in a higher order of photoemission in their case. In the meantime, a noticeable high photoelectron yield per pulse in Ref. [12] was obtained while a yield of less than one electron per pulse was achieved in our case. This is due to the fact that we intentionally control no more than one photoelectron per laser pulse to satisfy our electron spectra measurement requirement restricted by the delay line detector scheme in our experiment. In contrast, an imaging energy filter is used in Ref. [12], which is more suitable for obtaining the photoelectron energy spectrum with relatively large photoelectron flux. We limit the photoelectron number from one laser pulse excitation to avoid the influence of space charge effect on the photoelectron energy spectrum that is critical to judge the photoemission mechanism, as revealing the mechanisms of plasmon-induced

photoemission by comparing the discrepancy between PSP and LSP modes in the contribution to photoemission under ultrashort laser pulse excitation with photon energies well below the work function is one of the main concerns of the current paper.

#### IV. CONCLUSIONS

In conclusion, we have reported a nanoscale ultrafast electron emitter by focusing a PSP excited by circularly polarized light. It is found that with the same maximum photoemission intensity induced by the PSP and LSP the PSP induced photoemission in our case is dominated by an ATP process due to the absence of the radiative decay of the subradiation plasmonic mode, and the LSP induced one is, in contrast, dominated by thermally assisted multiphoton photoemission due to the existence of both radiative and nonradiative decay. Moreover, it is found that the PSP has unique advantages to facilitate photoelectron emission compared to the LSP even though the local field intensity is slightly lower since the photoemission intensity is contributed not only by near field intensity and duration time of a plasmon, but also the decay

channel of the plasmonic mode. This finding deepens our understanding of photoemission associated with plasmon effects and provides a chance to obtain an electron pulse with higher energy from a plane (reproducible emitter) structure without sharp nanostructures or protrusions. It is also important for establishing nanoscale femtosecond electron sources, which is a promising platform for several ambitious research endeavors ranging from ultrafast electron diffraction microscopy to free electron lasers.

#### ACKNOWLEDGMENTS

The authors acknowledge funding from National Natural Science Foundation of China (Grants No. 62005022, No. 61775021, No. 91850109, and No. 12004052), Department of Science and Technology of Jilin Province (Grants No. 20200201268JC and No. 20200401052GX), the “111” Project of China (Grant No. D17017), Key Laboratory of Ultrafast and Extreme Ultraviolet Optics of Jilin Province, Ministry of Education Key Laboratory for Cross-Scale Micro and Nano Manufacturing, and Changchun University of Science and Technology.

- 
- [1] R. K. Li, H. To, G. Andonian, J. Feng, A. Polyakov, C. Scoby, K. Thompson, W. Wan, H. Padmore, and P. Musumeci, Surface-Plasmon Resonance-Enhanced Multiphoton Emission of High-Brightness Electron Beams from a Nanostructured Copper Cathode, *Phys. Rev. Lett.* **110**, 074801 (2013).
- [2] R. G. Hobbs, Y. Yang, A. Fallahi, P. D. Keathley, E. D. Leo, F. X. Kärtner, W. S. Graves, and K. K. Berggren, High-yield, ultrafast, surface plasmon-enhanced, Au nanorod optical field electron emitter arrays, *ACS Nano* **8**, 11474 (2014).
- [3] A. Polyakov, C. Senft, K. F. Thompson, J. Feng, S. Cabrini, P. J. Schuck, H. A. Padmore, S. J. Peppernick, and W. P. Hess, Plasmon-Enhanced Photocathode for High Brightness and High Repetition Rate X-Ray Sources, *Phys. Rev. Lett.* **110**, 076802 (2013).
- [4] P. Hommelhoff, Y. Sortais, A. Aghajani-Talesh, and M. A. Kasevich, Field Emission Tip as a Nanometer Source of Free Electron Femtosecond Pulses, *Phys. Rev. Lett.* **96**, 077401 (2006).
- [5] H. Yanagisawa, S. Schnepf, C. Hafner, M. Hengsberger, D. E. Kim, M. F. Kling, A. Landsman, L. Gallmann, and J. Osterwalder, Delayed electron emission in strong-field driven tunnelling from a metallic nanotip in the multi-electron regime, *Sci. Rep.* **6**, 35877 (2016).
- [6] L. Wimmer, G. Herink, D. R. Solli, S. V. Yalunin, K. E. Echternkamp, and C. Ropers, Terahertz control of nanotip photoemission, *Nat. Phys.* **10**, 432 (2014).
- [7] E. Quinonez, J. Handali, and B. Barwick, Femtosecond photoelectron point projection microscope, *Rev. Sci. Instrum.* **84**, 103710 (2013).
- [8] C. Ropers, D. R. Solli, C. P. Schulz, C. Lienau, and T. Elsaesser, Localized Multiphoton Emission of Femtosecond Electron Pulses from Metal Nanotips, *Phys. Rev. Lett.* **98**, 043907 (2007).
- [9] S. Vilayurganapathy, M. I. Nandasiri, A. G. Joly, P. Z. El-Khoury, T. Varga, G. Coffey, B. Schwenzer, A. Pandey, A. Kayani, W. P. Hess, and S. Thevuthasan, Silver nanorod arrays for photocathode applications, *Appl. Phys. Lett.* **103**, 161112 (2013).
- [10] L. Wang and H. Petek, Focusing surface plasmon polariton wave packets in space and time, *Laser & Photonics Rev.* **7**, 1003 (2013).
- [11] C. Lemke, C. Schneider, T. Leibner, D. Bayer, J. W. Radke, A. Fischer, P. Melchior, A. B. Evlyukhin, B. N. Chichkov, C. Reinhardt, M. Bauer, and M. Aeschlimann, Spatiotemporal characterization of SPP pulse propagation in two dimensional plasmonic focusing devices, *Nano Lett.* **13**, 1053 (2013).
- [12] D. Podbiel, P. Kahl, A. Makris, B. Frank, S. Sindermann, T. J. Davis, H. Giessen, M. H. Hoegen, and F. J. Meyer zu Heringdorf, Imaging the nonlinear photoemission dynamics of electrons from strong plasmonic fields, *Nano Lett.* **17**, 6569 (2017).
- [13] B. Frank, P. Kahl, D. Podbiel, G. Spektor, M. Orenstein, L. Fu, T. Weiss, M. H. Hoegen, T. J. Davis, F.-J. Meyer zu Heringdorf, and H. Giessen, Short-range surface plasmonics: Localized electron emission dynamics from a 60-nm spot on an atomically flat single-crystalline gold surface, *Sci. Adv.* **3**, e1700721 (2017).
- [14] W. Chen, D. C. Abeyasinghe, R. L. Nelson, and Q. Zhan, Plasmonic lens made of multiple concentric metallic rings under radially polarized illumination, *Nano Lett.*, **9**, 4320 (2009).
- [15] Z. Fang, Q. Peng, W. Song, F. Hao, J. Wang, P. Nordlander, and X. Zhu, Plasmonic focusing in symmetry broken nanocorrals, *Nano Lett.* **11**, 893 (2010).
- [16] M. Müller, V. Kravtsov, A. Paarmann, M. B. Raschke, and R. Ernstorfer, Nanofocused plasmon-driven sub-10 fs electron point source, *ACS Photonics* **3**, 611 (2016).
- [17] A. Giugni, B. Torre, A. Toma, M. Francardi, M. Malerba, A. Alabastri, R. P. Zaccaria, M. I. Stockman, and E. Di Fabrizio, Hot-electron nanoscopy using adiabatic compression of surface plasmons, *Nat. Nanotechnol.* **8**, 845 (2013).

- [18] J. Pettine, P. Choo, F. Medeghini, T. W. Odom, and D. J. Nesbitt, Plasmonic nanostar photocathodes for optically-controlled directional currents, *Nature Commun.* **11**, 1367 (2020).
- [19] G. Wang, X. Song, P. Lang M. Jiang, B. Ji, Z. Fang, and J. Lin, Fano resonance enhanced multiphoton photoemission from single plasmonic nanostructure excited by femtosecond laser, *Phys. Rev. B* **103**, 155403 (2021).
- [20] J. Lehmann, M. Merschdorf, W. Pfeiffer, A. Thon, S. Voll, and G. Gerber, Surface Plasmon Dynamics in Silver Nanoparticles Studied by Femtosecond Time-Resolved Photoemission, *Phys. Rev. Lett.* **85**, 2921(2000).
- [21] M. Merschdorf, W. Pfeiffer, A. Thon, S. Voll, and G. Gerber, Photoemission from multiply excited surface plasmons in Ag nanoparticles, *Appl. Phys. A* **71**, 547 (2000).
- [22] Y. Dai, and H. Petek, Plasmonic spin-Hall effect in surface plasmon polariton focusing, *ACS Photonics* **6**, 2005 (2019).
- [23] P. B Johnson and R. W. Christy, Optical constants of the noble metals, *Phys. Rev. B* **6**, 4370. (1972).
- [24] Y. Dai, M. Dabrowski, V. A. Apkarian, and H. Petek, Ultrafast microscopy of spin momentum-locked surface plasmon polaritons, *ACS Nano* **12**, 6588 (2018).
- [25] M. Aeschlimann, C. A. Schmuttenmaer, H. E. Elsayed-Ali, R. J. D. Miller, J. Cao, Y. Gao, and D. A. Mantell, Observation of surface enhanced multiphoton photoemission from metal surfaces in the short pulse limit, *J. Chem. Phys.* **102**, 8606 (1995).
- [26] H. B. Michaelson, Work function of elements and its periodicity, *J. Appl. Phys.* **48**, 4729 (1977).
- [27] T. Kaiser, M. Falkner, J. Qi, A. Klein, M. Steinert, C. Menzel, C. Rockstuhl, and T. Pertsch, Characterization of a circular optical nanoantenna by nonlinear photoemission electron microscopy, *Appl. Phys. B* **122**, 1 (2016).
- [28] M. Schenk, M. Kruger, and P. Hommelhoff, Strong-Field Above-Threshold Photoemission from Sharp Metal Tips, *Phys. Rev. Lett.* **105**, 257601 (2010).
- [29] See Supplemental Material at <http://link.aps.org/supplemental/10.1103/PhysRevB.104.155432> for (1) the calculated near field enhancement spectrum of the hot spot on the rim by FDTD; (2) the PEEM images of the lens illuminated by right-circularly polarized light, left-circularly polarized light, and linearly p-polarized light; (3) the photoelectron spectra; and (4) the reconstructed image by considering the temporal integral of the sixth power of the instantaneous electric field.
- [30] <https://support.lumerical.com/hc/en-us/articles/360034382894-Understanding-injection-angles-in-broadband-simulations>.
- [31] A. Grubisic, S. Mukherjee, N. Halas, and D. J. Nesbitt, Anomalous strong electric near-field enhancements at defect sites on Au nanoshells observed by ultrafast scanning photoemission imaging microscopy, *J. Phys. Chem. C* **117**, 22545 (2013).
- [32] Y. Gong, A. G. Joly, P. Z. El-Khoury, and W. P. Hess, Polarization-directed surface plasmon polariton launching, *J. Phys. Chem. Lett.* **8**, 49 (2017).
- [33] Y. Qin, B. Ji, X. Song, and J. Lin, Ultrafast spatiotemporal control of directional launching of surface plasmon polaritons in a plasmonic nano coupler, *Photonics Res.* **9**, 514 (2021).
- [34] M. Lehr, K. Bley, N. Vogel, B. Rethfeld, G. Schönhense, and H. J. Elmers, Evidence of spatially inhomogeneous electron temperature in a resonantly-excited array of bow-tie nanoantennas, *J. Phys. Chem. C* **123**, 12429 (2019).
- [35] G. Banfi, G. Ferrini, M. Peloi, and F. Parmigiani, Anomalous photoemission from Ag(100) in the femtosecond regime, *Phys. Rev. B* **67**, 035428 (2003).
- [36] Z. Lin and L. V. Zhigilei, Electron-phonon coupling and electron heat capacity of metals under conditions of strong electron-phonon nonequilibrium, *Phys. Rev. B* **77**, 075133 (2008).
- [37] A. Grubisic, V. Schweikhard, T. A. Baker, and D. J. Nesbitt, Coherent multiphoton photoelectron emission from single Au nanorods: The critical role of plasmonic electric near-field enhancement, *ACS Nano* **7**, 87 (2013).
- [38] L. V. Keldysh, Diagram technique for nonequilibrium processes, *Sov. Phys. JETP* **20**, 1307 (1965).
- [39] P. Melchior, D. Bayer, C. Schneider, A. Fischer, M. Rohmer, W. Pfeiffer, and M. Aeschlimann, Optical near-field interference in the excitation of a bowtie nanoantenna, *Phys. Rev. B* **83**, 235407 (2011).
- [40] M. Aeschlimann, M. Bauer, D. Bayer, T. Brixner, F. J. Garcia de Abajo, W. Pfeiffer, M. Rohmer, C. Spindler, and F. Steeb, Adaptive subwavelength control of nano-optical fields, *Nature (London)* **446**, 301 (2007).
- [41] Q. Sun, H. Yu, K. Ueno, A. Kubo, Y. Matsuo, and H. Misawa, Dissecting the few-femtosecond dephasing time of dipole and quadrupole modes in gold nanoparticles using polarized photoemission electron microscopy, *ACS Nano* **10**, 3835 (2016).
- [42] Y. Xu, Y. Qin, B. Ji, X. Song, and J. Lin, Polarization manipulated femtosecond localized surface plasmon dephasing time in an individual bowtie structure, *Opt. Express* **28**, 9310 (2020).
- [43] S. A. Maier, *Plasmonics: Fundamentals and Applications* (Springer, New York, 2007).
- [44] C. Sönnichsen, T. Franzl, T. Wilk, G. von Plessen, and J. Feldmann, Drastic Reduction of Plasmon Damping in Gold Nanorods, *Phys. Rev. Lett.* **88**, 077402 (2002).
- [45] M. Aeschlimann, T. Brixner, M. Cinchetti, B. Frisch, B. Hecht, M. Hensen, B. Huber, C. Kramer, E. Krauss, T. H. Loeber, W. Pfeiffer, M. Piecuch, and P. Thielen, Cavity-assisted ultrafast long-range periodic energy transfer between plasmonic nanoantennas, *Light-Sci. Appl.* **6**, e17111 (2017).
- [46] L. Douillard, F. Charra, Z. Korczak, R. Bachelot, S. Kostcheev, G. Lerondel, P. M. Adam, and P. Royer, Short range plasmon resonators probed by photoemission electron microscopy, *Nano Lett.* **8**, 935 (2008).
- [47] C. Clavero, Plasmon-induced hot-electron generation at nanoparticle/metal-oxide interfaces for photovoltaic and photocatalytic devices, *Nat. Photonics* **8**, 95 (2014).
- [48] T. E. Furtak and J. K. Sasser, Crystallographic anisotropy in the decay of surface plasmons to photoelectrons, *Surf. Sci.* **78**, 591 (1978).
- [49] B. Rethfeld, A. Kaiser, M. Vicanek, and G. Simon, Ultrafast dynamics of nonequilibrium electrons in metals under femtosecond laser, *Phys. Rev. B* **65**, 214303 (2002).
- [50] A. Gloskovskii, D. Valdaitsev, S. A. Nepijko, G. Schönhense, and B. Rethfeld, Coexisting electron emission mechanisms in small metal particles observed in fs-laser excited PEEM, *Surf. Sci.* **601**, 4706 (2007).